Materials Horizons

ROYAL SOCIETY OF CHEMISTRY

COMMUNICATION

View Article Online
View Journal | View Issue

Cite this: *Mater. Horiz.*, 2024, 11, 3633

Received 18th February 2024,
Accepted 13th May 2024

DOI: 10.1039/d4mh00172a

rsc.li/materials-horizons

Wood waste-derived dual-mode materials paving the way for year-round energy saving in buildings†

Jiayi Zhang, Kairen Yin, Zirui Zhuang, Jinghan Zhou, Yixi Tang, Jingyong Xu, Yipeng Chen, * Yingying Li* and Qingfeng Sun *

In the face of the challenges posed by global warming, traditional methods of building heating and cooling contribute significantly to electricity and coal consumption, thereby emitting considerable amounts of greenhouse gases. Here, a dual-mode thermal management structural material is created by processing sustainable cellulose and lignin derived from wood waste into gels, followed by lamination. The cellulose surface of the material exhibits the ability to scatter solar radiation backward while emitting strongly in the mid-infrared wavelengths, whereas the lignin surface absorbs visible and near-infrared light, primarily releasing energy through non-radiative transitions. Consequently, the material can achieve sub-ambient radiative cooling of 6 °C and solar heating of 27.5 °C during the daytime by simply flipping its orientation. This pioneering material showcases the potential to significantly reduce cooling energy consumption by an average of 18% and heating energy consumption by 42%. Moreover, the integration of a thermal-electric generator within the dual-layer structure optimally utilizes the temperature differential between the two layers, converting it into electrical power. Notably, the dual-mode thermal management structural material exhibits impressive mechanical strength, boasting a flexural strength of 102 MPa, surpassing that of natural wood by over 4.8 times. With its dual-mode functionality and embedded thermal-electric generator, this material represents a crucial step towards achieving both thermal comfort and energy autonomy in sustainable building practices, thereby contributing to a more environmentally friendly and efficient future.

New concepts

We have demonstrated a novel concept of dual-functional structural material derived from renewable wood waste. This material combines passive temperature regulation with electricity generation capabilities, offering a sustainable solution for energy-efficient buildings. What sets our concept apart from existing research is its dual functionality and the utilization of renewable wood waste. While previous studies have focused on single-purpose materials, our material offers both cooling and heating functions, depending on the environmental conditions. Furthermore, by utilizing wood waste, we contribute to a circular economy, reducing waste and providing a cost-effective alternative to traditional materials. Our work and the underlying concept bring valuable insights to materials science. It demonstrates the potential of renewable resources in creating advanced materials with dual functionalities. Additionally, it highlights the need to reconsider waste as a resource for innovative material development, leading to more sustainable and efficient solutions in the future.

Introduction

Building energy consumption constitutes over 30% of total global greenhouse gas emissions and 10% of global energy use, posing significant environmental and economic challenges.[1,2] In the United States, approximately fifteen percent of total energy consumption is allocated to heating and cooling buildings.[3] Moreover, projections indicate a substantial increase in home heating and cooling energy demands from 0.8 Gt C in 2000 to around 2.2 Gt C by 2100, driven by population growth, economic expansion, and climate change.[2,4] To address this escalating trend and promote global sustainability, the adoption of green passive radiation energy-saving structural materials is crucial.

While current research primarily focuses on developing single-function structural materials,[5,6] it is imperative to recognize the inherent variability in diurnal, seasonal, climatic zones, and other environmental fluctuations that buildings encounter.[4,7,8] Analyzing historical data of residential degree-days, such as those in Oklahoma City from 1981 to 2010, reveals that the number of residential degree-days for heating and cooling was 3365 and 2098, respectively.[8] Analyzing historical data of residential degree-days, such as those in Oklahoma City from 1981 to 2010, reveals that the number of residential degree-days for heating and cooling was 3365 and 2098, respectively.

College of Chemistry and Materials Engineering, Zhejiang A&F University, Hangzhou, Zhejiang Province, 311300, P. R. China. E-mail: zafucyp@163.com, yyli@zafu.edu.cn, qfsun@zafu.edu.cn

† Electronic supplementary information (ESI) available. See DOI: https://doi.org/10.1039/d4mh00172a

Wood, boasting a millennia-spanning legacy, has emerged as a pivotal sustainable building material, capitalizing on its economic and environmental advantages. The primary constituents of wood, cellulose, and lignin, represent the world's largest biomass resource and exhibit unique optical properties. Cellulose fibers, known for their non-absorption in the visible range yet strong infrared emission attributable to molecular vibration and stretching, provide a solid foundation for structural integrity.[6,9] Conversely, lignin, distinguished by its rich aromatic rings and conjugated functional groups, fosters robust conjugation and π–π molecular interactions among lignin molecules.[10,11] This distinctive molecular composition affords lignin exceptional optical characteristics, including aggregation-induced emission and UV absorbance, rendering it highly conducive to sustainable photothermal conversion.[12,13] The unique optical attributes of cellulose and lignin from wood substrates position them as ideal candidates for passive heating and cooling structural materials.[1,14] In recent years, there has been a surge of interest in developing innovative wood-based materials for thermal regulation in buildings. These materials, including lignin-based photothermal,[10,11] cellulose-based radiative cooling materials,[5,15] and phase change energy storage wood,[16,17] offer unique solutions for enhancing energy efficiency and sustainability in architectural design. By harnessing the inherent properties of wood and incorporating advanced fabrication techniques, researchers have achieved remarkable progress in enhancing solar energy utilization, radiative cooling, and temperature control. These studies have the potential to revolutionize the field of architectural engineering, providing practical solutions for addressing global challenges associated with climate change and energy consumption.

However, the sourcing of cellulose and lignin from wood processing residues often encounters significant challenges in wastage and underutilization. In 2018, recycled municipal waste wood in the United States amounted to 3.1 million tons, representing a mere 17% of total waste wood, emphasizing the imperative of extracting lignocellulose through the reuse of recycled wood as an economically and environmentally viable solution (Fig. 1a and b).[18] Similarly, Finland has faced comparable challenges in recent years (Fig. S1, ESI†),[19] with wood playing a significant role in recycled materials utilization[20] (Fig. S2, ESI†).[15]

Here, a strategy utilizing recycled wood demonstrated the creation of a dual-mode thermal managing structural (TMS) material, enabling efficient year-round radiative temperature regulation. This material was derived from lignocellulosic pulping products, where cellulose and lignin underwent separate pretreatment to form gels, followed by densification using lamination techniques. Notably, the distinctive molecular structures of cellulose and lignin govern the dual-mode TMS material's thermal management capabilities, overseeing radiative cooling and photothermal conversion processes, respectively. With exceptional optical properties, this material achieves a cooling power density of up to 52.5 W m^{-2} and daytime heating of 27.5 °C. Moreover, functional applications, such as photothermal generators, leverage the temperature differential generated by the material's radiative cooling and

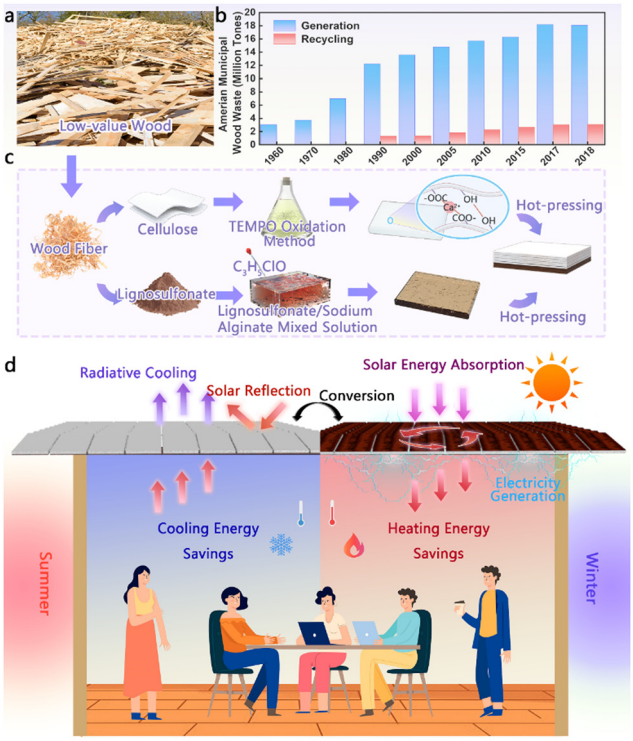

Fig. 1 Preparation of high-performance dual-mode TMS material and concept illustration. (a) Photograph showing waste wood. (b) The total generation and recycling of municipal wood waste. (c) Delignification of recovered wood fibers to extract cellulose and lignin sulfonate. Cellulose hydrogels and lignin hydrogels were prepared on this industrial basis by our bottom-up approach, and hot press dried to make dual-mode TMS material. (d) The optical properties of the dual-mode TMS material are engineered to be high emissivity and photothermal conversion of solar power. In the atmospheric window, the cellulose surface has a high emissivity to increase the rate of radiative heat exchange in a hot environment. The cellulose surface is also highly reflective in the solar spectrum, further reducing solar energy gain during the summer. The lignin surface converts the absorbed solar energy into thermal and electric energy, as well as warms the room in winter.

photothermal conversion. Furthermore, its mechanical properties meet the stringent requirements of advanced structural materials, boasting a flexural strength of 102 MPa, surpassing pure wood bulk by 4.8 times in mechanical strength and toughness. By seamlessly integrating heating management, thermal insulation, and high performance, this innovation paves the way for a sustainable and energy-efficient future in advanced thermal management structural materials. This paradigm-shifting advancement not only diverges from conventional approaches but also heralds a transition towards a greener, more sustainable construction industry.

Results and discussion

Preparation strategy of the dual-mode thermal management structural material

The dual-mode structure is pivotal in realizing the experimental implementation of the dual-mode thermal management

structural material. Fig. 1c illustrates the schematic process of fabricating the dual-mode TMS material using wood waste as the raw material. Initially, lignocellulose and lignosulfonate were obtained separately through conventional papermaking techniques (Fig. S3, ESI†).[21] Subsequently, cellulose underwent oxidation *via* the tempo oxidation method[22,23] to convert the hydroxyl group (–OH) to carboxyl group (–COOH) on its surface (Fig. S4, ESI†).[24,25] Concurrently, lignosulfonate and sodium alginate were thoroughly mixed and cross-linked by the addition of epoxy chloropropane to form numerous ether bonds within the precursor (Fig. S5, ESI†).[1,26] The oxidized cellulose and precursor were then immersed in a $CaCl_2$ solution for cross-linking and replacement, yielding cellulose hydrogels and lignosulfonate hydrogels. Finally, multiple layers of cellulose hydrogels and lignosulfonate hydrogels were subjected to hot-pressing to produce a high-performance dual-mode TMS material.

As illustrated in Fig. 1d, the dual-mode TMS material comprises a double-sided composite consisting of cellulose and lignin substrates, offering simultaneous solar heating and radiative cooling functionalities. Owing to the material's cooling segment's pronounced whiteness, it predominantly reflects sunlight. Additionally, the material exhibits excellent infrared emissivity within the atmospheric window (8–13 μm), facilitating high thermal radiation levels that directly impact the roof, enabling passive sub-ambient cooling.[6,27,28] According to the radiative heat flow formula from the material to the surrounding environment (Supplementary Notes 2, ESI†), the thicker cellulose layer enhances heat dissipation from the indoor environment, thereby augmenting the cooling effect. The dual-mode transition is achieved through a novel reversible tile structure (Fig. S6, ESI†). During the heating mode, lignin absorbs most of the solar energy, converting it into heat energy, thereby enabling efficient daytime heating.[29,30] Conversely, positioning the thinner solar absorption layer (lignin surface) outward increases the distance between it and the indoor environment, reducing thermal conductivity (Fig. S7, ESI†). This asymmetric thickness dual-mode design considers the material's operational mechanisms and heat transfer characteristics in different modes, enhancing its overall performance. Furthermore, integrating a thermoelectric module into the dual-mode TMS material facilitates the creation of a solar thermoelectric generator. This innovative system leverages the temperature differential between the heating and cooling surfaces to generate electricity, thereby contributing to energy conservation and offering concurrent energy harvesting capabilities.

Morphology of the dual-mode thermal management structural material

To experimentally demonstrate the dual-mode functionality of the TMS material, the microstructure of the bilayer material is of paramount importance. Unlike fiberboard composed of irregular fibers, the constituents in the dual-mode TMS material (cellulose and lignin) are nearly at the nanometer scale and are densely compacted under hot pressing treatment (Fig. 2a and b), enhancing the toughness and strength of the structural material compared to a microstructure characterized by loose and highly porous features (Fig. 2d and e). Fig. 2c illustrates the

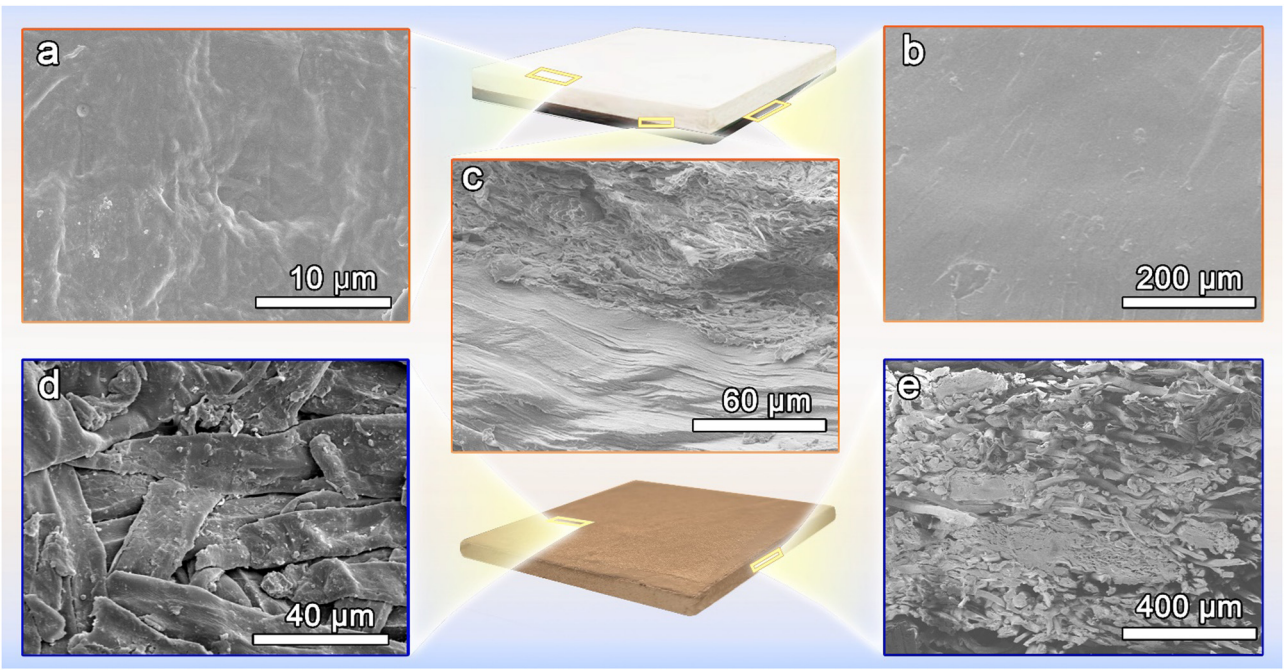

Fig. 2 The structural characterization of dual-mode TMS material and wood fiber bulk. (a) The smooth, compact surface of the cooling surface (cellulose surface). (b) The smooth, compact surface of the heating surface (lignin surface). (c) The SEM magnification of the cooling side shows the microscopic laminated structure. The laminated structure of the heating side can be seen using SEM magnification. And the cooling layer and the heating layer are tightly fitted together. (d) Optical microscope image of the wood fiber bulk showing rough wood fibers. (e) The loose structure of the wood fiber bulk is filled with pores.

laminated structure of the dual-mode TMS material, where cellulose and lignin intertwine extensively within the layers and are bonded together by robust hydrogen bonds.[31]

Mechanical properties of the dual-mode thermal management structural material

The dual-mode TMS material, serving as a structural component, must satisfy specific mechanical strength requirements. Fig. 3a depicts the stress–strain curves of the dual-mode TMS material compared to those of pure wood fiber bulk. The initial decrease in stress is attributed to the initiation and propagation of cracks within the material, leading to a decrease in load-bearing capacity. Subsequently, the increase in stress is associated with mechanisms such as crack bridging, fiber reorientation, or interfacial interactions between the layers, which contribute to the material's ability to withstand higher loads. The flexural strength of the dual-mode TMS material reaches an impressive 102 MPa, marking a fivefold increase over that of the pure wood fiber bulk. Moreover, the dual-mode TMS material demonstrates exceptional performance in impact toughness, achieving 72.32 kJ m^{-2}, surpassing traditional structural materials such as hooked steel fiber concrete and silicon nitride ceramic, while quadrupling that of the pure wood fiber bulk (Fig. 3b). Typically, materials with high toughness and strength exhibit a trade-off relationship.[32] However, the dual-mode TMS material defies this convention by concurrently offering both high toughness and high strength. To comprehensively illustrate the mechanical properties of the dual-mode TMS material, a performance chart is employed to compare its characteristics with those of other structural materials (Fig. 3c). Notably, owing to the low density of wood-based materials, the dual-mode TMS material occupies a distinct domain characterized by high specific strength (76.86 MPa g^{-1} cm^3) and specific impact toughness (53.96 kJ m^{-2} g^{-1} cm^3), surpassing various structural materials and polymers. This spectrum of mechanical properties positions the dual-mode TMS material as an exemplary high-performance and lightweight structural material.

The findings of the aforementioned study validate the effectiveness of our lignocellulosic design in enhancing mechanical properties. During the fabrication of the dual-mode TMS material, a multilayer structure was achieved through hot pressing, endowing the material with both high toughness and strength. This unique toughened structure is evident in the stress–strain curve: The dual-mode TMS material has a multilayer structure composed of lignin substrate and cellulose substrate. During the process of separating lignin from cellulose (cooking and bleaching), the breaking of various bonds (such as ether bonds, carbon–carbon double bonds, *etc.*) leads to the fragmentation of large molecules.[33] Conversely, TEMPO-mediated oxidation of cellulose can retain a good fiber morphology. Therefore, when subjected to external loads, certain lignin layers in the dual-mode TMS material may fracture prior to the cellulose layers connected by microfibers on the fiber surface.[34] Thus, at a strain of approximately 1.2, the dual-mode TMS material briefly exhibits a trough. Following the initial fracture, a series of cracks expand/layer within the lignin layer, gradually reducing stress. This fracture behavior indicates that the material possesses high deformation resistance.[35] Unlike pure wood fiber bulk, internal deformation persists even after initial bending occurs. When subjected to bending forces, the layers of the dual-mode TMS material experience sliding, causing firmly hydrogen-bonded fibers at the interface to be pulled out from the adjacent layer (Fig. 3d–f and Fig. S8a, ESI†), which are coincident with the simulated crack propagation behavior (Fig. S8b, ESI†).

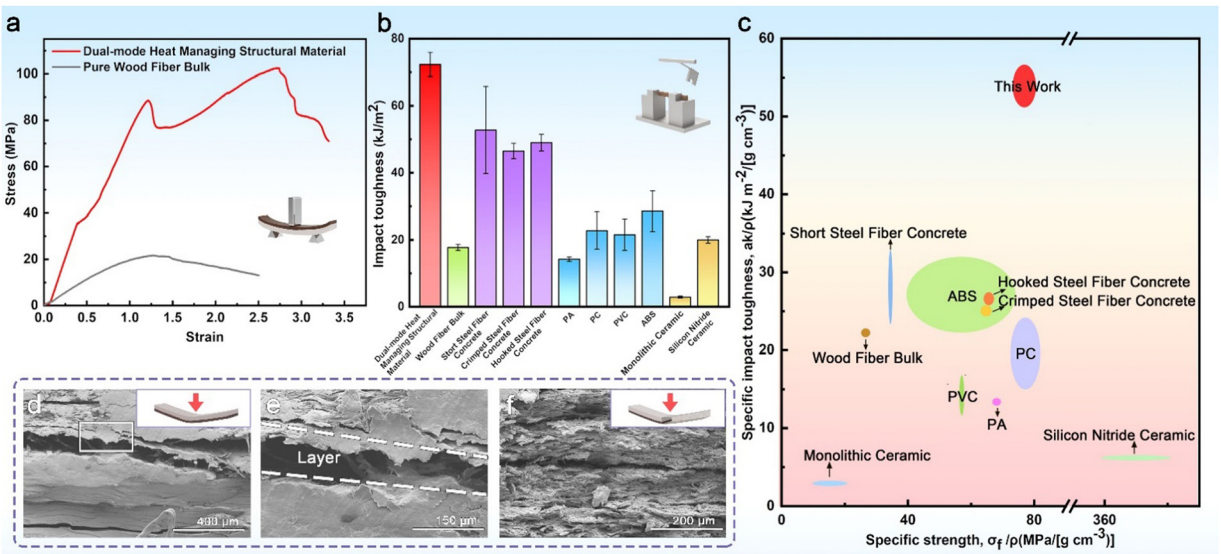

Fig. 3 The mechanical properties and characterization of dual-mode TMS material. (a) The flexural stress–strain test of dual-mode TMS materials and wood fiber bulk. (b) Impact toughness of dual-mode TMS material compared to common structural materials and polymers. (c) Performance charts comparing mechanical properties of dual-mode TMS material with other materials.[41–47] (d) Profile of a cracked dual-mode TMS material demonstrating layer-to-layer sliding. (e) Numerous fibers are entangled among layers [enlarger micrograph of the region shown in (d)]. (f) The longitudinal section of a dual-mode TMS material fractured under external pressure, clearly showing the fibers pulled out due to the slip of the force.

Consequently, stress is dispersed, mitigating crack initiation and propagation.[36] Owing to the abundance of hydroxyl groups within the layers, deformation of the dual-mode TMS material prompts relative sliding between layers, accompanied by the creation, disruption, and reformation of a vast number of hydrogen bonds (Fig. S9, ESI†).[37] This phenomenon contributes to superior strength and durability compared to other structural materials.[3,38–40]

Optical properties and mechanisms of the dual-mode thermal management structural material

For the dual-mode TMS material, the effective radiative cooling/heating capability is the most important property. For radiative cooling, having a high emissivity in the atmospheric window means that more heat can be radiated away from the environment. The diffuse gold integrating sphere is used to test the emissivity of materials using FTIR spectroscopy (Fig. 4a). The cooling surface has a significant emittance and mainly arises from cellulose molecules' vibration and stretching (Fig. 4b). The heating surface also exhibits a high emissivity similar to that of the cooling surface, owing to the amorphous nature of lignin, which is composed of phenylpropane polymers. Lignin possesses strong infrared thermal emission capabilities and exhibits significant molecular vibrations in the mid-infrared range.[48,49] The cooling surface radiate a net heat flux through the atmospheric transparency window (8 to 13 mm) to the cold sink of outer space in the form of infrared radiation. And cooling surface exhibits high emissivity (similarly greater than 0.9) in the infrared range, emitting strongly between 60 degrees, indicating a stable heat flow density release when the relative angle of the cooling surface to the sky is different, which 10% higher than formerly reported values (Fig. 4c).[50,51] In the solar spectrum, the heating surface displayed a distinctive single-band absorption pattern, with the peak absorption occurring at approximately 353 nm. This absorption profile is attributed to the characteristic absorption of benzene rings present in lignin. Despite a gradual decrease in light absorption with increasing wavelength, significant absorption persisted at 808 nm. This implies that both visible light and near-infrared (NIR) light can serve as effective illumination sources for the photothermal conversion of lignin (Fig. 4d). The high, diffusive reflectance of the cooling surface has caused almost 95 percent of the solar irradiation to be reflected (Fig. 4e). And our dual-mode TMS material has a lower thermal conductivity, which makes it have stronger thermal insulation ability (Fig. S7, ESI†). In contrast, the heating surface is black in the solar spectrum. The heating surface is rich in lignin, which, as an aromatic compound, after the lignin absorbed near-infrared light, the π–π conjugated structure in lignin molecules facilitated the electronic transition from a low-energy ground state (S_0) to the excited state (S_1).[52] At the same time, due to the fiber and multi-layer structure, light diffuses and refracts inside the

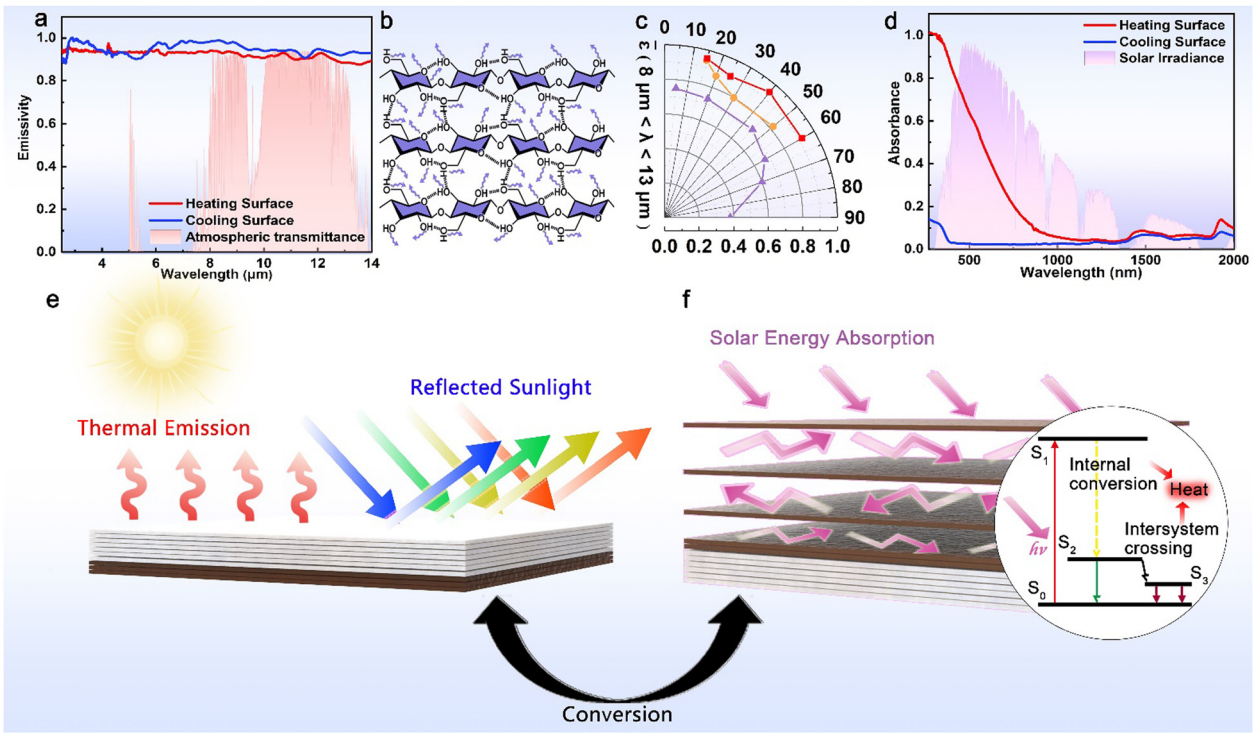

Fig. 4 Optical measurement and characterization of dual-mode TMS material. (a) The emissivity of heating surface and cooling surface are measured by FTIR equipped with a diffuse gold integrating sphere. (b) Diagram of infrared emission *via* vibration of the functional groups of cellulose. (c) The average emissivity across angles of the cooling surface. (d) The ultraviolet-to-near-infrared wavelength absorption of heating and cooling surfaces. The region represented by the color mauve is the solar spectral irradiance. (e) Schematic demonstrating that the cooling surface reflects solar radiation significantly. (f) The heating surface exhibited high ultraviolet absorption and converted into heat energy for indoor heating.

heated wood structure material, which enhances the absorption and conversion of light energy (Fig. 4f).[29,53] These unique optical properties provide the basis for practical applications of dual-mode TMS material.

Thermal management performance of the dual-mode thermal management structural material

The experiment involved observing the photothermal conversion process of the heating surface under 808 nm near-infrared (NIR) laser irradiation. Subsequently, an infrared imager was utilized to monitor the temperature changes in the composites (Fig. 5a). As illustrated in Fig. 5b, the maximum temperature (T_{max}) of the heating surface demonstrated a proportional increase in response to the light power density, escalating from 55.5 °C (0.10 W cm^{-2}) to 201 °C (1.0 W cm^{-2}). This highlights the ability to precisely control Tmax by adjusting the light power density. Conversely, pure sodium alginate film (devoid of lignin) exhibited negligible photothermal effects (Fig. S10, ESI†), emphasizing the essential role of lignin in the photothermal conversion of the composite material.

To evaluate the outdoor performance of our dual-mode thermoregulating material system (TMS) in terms of solar heating and radiative cooling, we conducted tests using two sets of 100 mm by 100 mm dual-mode TMS material placed in parallel within two thermal boxes for direct temperature monitoring (Fig. 5c). These thermal boxes were positioned on a sunny platform, elevated 1 m above the surface to prevent heat transmission from the terrace's surface to the inside of the boxes (Fig. S11, ESI†). During a warm summer day, we assessed the heating/cooling performance of the dual-mode TMS material by comparing the steady-state temperature of our samples to the ambient air temperature (Fig. 5d). Solar irradiance data for the day of the outdoor test is provided in Fig. S12 (ESI†). The radiative cooling power was measured as the energy produced by electric heating when the surface temperature of the specimen was maintained at the same level as the surrounding temperature. In a parallel box with identical samples, we demonstrated radiative cooling power, achieving a remarkable cooling power of 52.5 W m^{-2} (Fig. S13, ESI†). Upon switching off the heaters, the cooling mode exhibited effective cooling of 6 °C and 9.4 °C throughout the day and night, respectively. Compared to ordinary structural materials such as concrete or ceramic, our samples exhibited significantly enhanced maximum temperature difference (27.5 °C) during the daytime compared to the ambient temperature (Fig. S14, ESI†). The data from these tests provide clear evidence of the effectiveness of our dual-mode TMS material as a temperature-regulating material, showcasing its potential for practical applications in real-world settings.

To evaluate the outdoor performance of our dual-mode thermoregulating material system (TMS) in terms of solar heating and radiative cooling, we conducted tests using two sets of 100 mm by 100 mm dual-mode TMS material placed in parallel within two thermal boxes for direct temperature monitoring (Fig. 5c). These thermal boxes were positioned on a sunny platform, elevated 1 m above the surface to prevent heat transmission from the terrace's surface to the inside of the boxes (Fig. S11, ESI†). During a warm summer day, we assessed the heating/cooling performance of the dual-mode TMS material by comparing the steady-state temperature of our samples to the ambient air temperature (Fig. 5d). Solar irradiance data for the day of the outdoor test is provided in Fig. S12 (ESI†). The radiative cooling power was measured as the energy produced by electric heating when the surface temperature of the specimen was maintained at the same level as the surrounding temperature. In a parallel box with identical samples, we demonstrated radiative cooling power, achieving a remarkable cooling power of 52.5 W m^{-2} (Fig. S13, ESI†). Upon switching off the heaters, the cooling mode exhibited effective cooling of 6 °C and 9.4 °C throughout the day and night, respectively. Compared to ordinary structural materials such as concrete or ceramic, our samples exhibited significantly enhanced maximum temperature difference (27.5 °C) during the daytime compared to the ambient temperature (Fig. S14, ESI†). The data from these tests provide clear evidence of the effectiveness of our dual-mode TMS material as a temperature-regulating material, showcasing its potential for practical applications in real-world settings.

Incorporating a thermoelectric module into the cooling and heating layer leads to the development of a solar thermoelectric generator (TEG), as illustrated in Fig. 6a. The processes involved in heat flow generation, transmission, and utilization

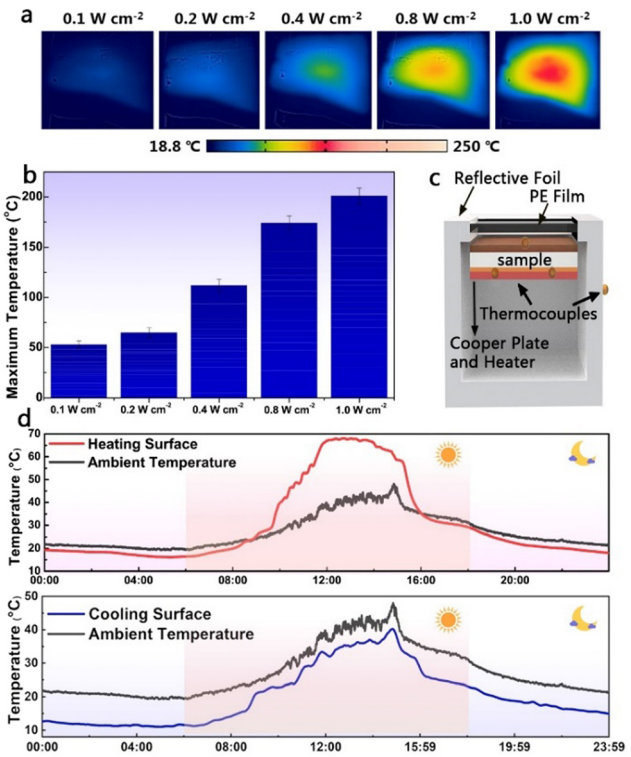

Fig. 5 (a) Infrared thermal imaging images and (b) surface maximum temperature of heating surface irradiated under different light power densities. (c) A diagram of the thermal box was used to quantify the temperature. (d) A continuous twenty-four-hour monitoring of the surface temperature of a dual-mode TMS material and the ambient temperature.

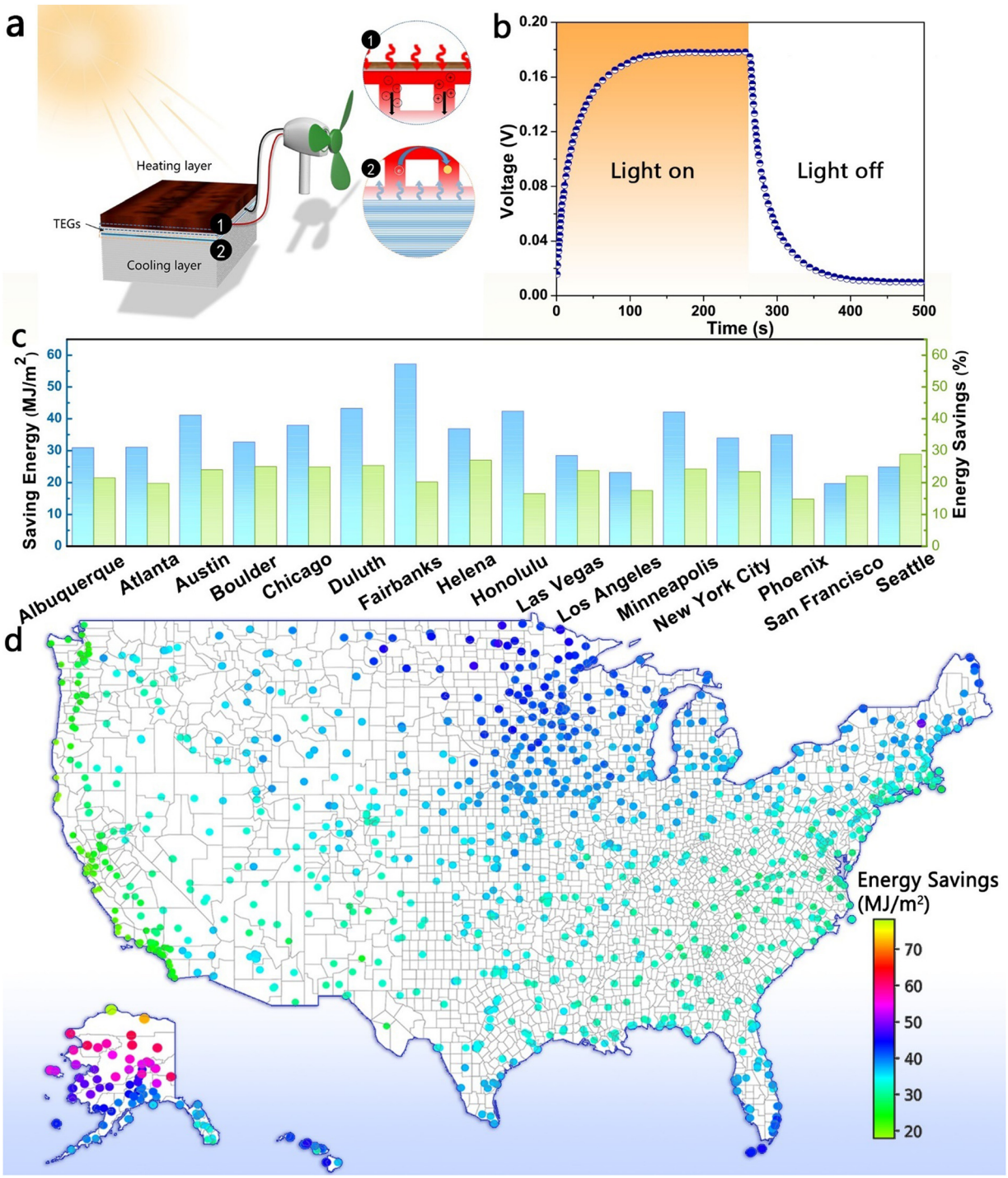

Fig. 6 (a) Schematic illustration for the solar thermal generator, heat flows through the top and bottom layers of TEG (lebeled as 1 and 2, respectively) during the operation. (b) The voltage generated by the solar TEG device when the light was turned on/off (0.10 W cm^{-2}). (c) Total cooling and heating energy savings percentage and per year among all 16 cities. (d) Energy-savings map of the United States illustrating the installation of dual-mode TMS materials on the roof of a typical midrise apartment complex.

within the solar TEG can be delineated into two distinct steps (as shown in the inset of Fig. 6a): (1) the heating layer converts sunlight into heat, acting as the primary energy input, and directs this heat through the TEG for electricity generation, and (2) the cooling layer decreases the temperature of the cold side of the TEG, thereby enhancing electricity generation. Infrared images of the dual-mode material under 0.1 W cm^{-2} illumination were captured, revealing a distinct temperature gradient from the top surface of the heating layer to the bottom of the cooling layer after 1 hour of irradiation (Fig. S15, ESI†). Subsequently, a voltage of approximately 0.18 V and an output current of 31.7 mA were generated (Fig. 6b and Fig. S16, ESI†).

The dual-mode material demonstrated sensitivity to light, as the voltage could be rapidly reduced by turning off the light source. Moreover, the voltage generated by the TEG exhibited a clear dependence on light intensity, increasing from 0.12 V to 0.22 V with the rise in light intensity (Fig. S17, ESI†). This electric energy generated by the dual-mode material has practical applications; for instance, it can power an electric fan (Movie S1, ESI†), demonstrating the conversion of lighting into readily usable electric energy.

Our dual-mode material effectively regulates room temperature by switching between modes (Movie S2, ESI†). To quantitatively assess the potential impact of our dual-mode material on building energy efficiency, we employed EnergyPlus version 8 and empirical material performance data to simulate the potential energy savings associated with using dual-mode thermal management structural material on building roofs. This study utilized models of mid-rise apartment complexes across the United States to evaluate the annual energy savings achievable with a dual-mode building envelope (Fig. S18, ESI†).[54] The interior boundary conditions were set with an interior set-point temperature of 18 °C in winter and 26 °C in summer, while the exterior boundary conditions utilized hourly weather data for a typical meteorological year. We selected 16 cities representing the 16 climate zones of the United States to generalize the study findings nationwide. The energy savings and percentages for these 16 cities relative to the baseline under dual-mode energy savings are presented in Fig. 6c. On average, mid-rise apartments across the 16 cities can achieve approximately 22.4% total energy savings. Notably, northern and central U.S. cities exhibit significant energy savings impacts. For instance, Seattle and Boulder were able to save 28.83% and 25.06% of their cooling and heating energy, respectively. This can be attributed to the climatic characteristics of these regions, which necessitate heating and cooling regulation throughout the year. The extended and dry winters allow the heating mode to fully leverage its advantages in capturing sunlight and converting light energy into heat to warm the room. Meanwhile, the uninterrupted 24-hour cooling mode effectively counteracts the short, hot summers. Based on our simulations, the overall cooling and heating energy savings from implementing this dual-mode installation can reach 22.86% (Fig. 6d). On average, this translates to 18% reduction in cooling energy consumption and 42% reduction in heating energy consumption, contributing significantly to the reduction of the building's carbon footprint from energy consumption (Fig. S19, ESI†). Compared to other similar materials, our dual-mode material demonstrates significant potential in thermal management performance (Table S1, ESI†).

Based on our comprehensive testing of the dual-mode material properties, including porosity, acoustic properties, water resistance, and optical performance after bending (Fig. S20–S22, ESI†), we have concluded that our material is well-suited for applications in the construction industry. These test results demonstrate that our material meets the requirements of construction materials, providing a reliable solution for architectural design and engineering. These findings will drive further advancements in materials science and contribute substantively to sustainable architecture and environmental conservation.

Conclusions

A dual-mode thermal management system (TMS) material, derived from residual products of wood pulp processing, namely cellulose and lignin, has been successfully developed. This material can be produced through a scalable batch process to exhibit a distinctive spectral response. Specifically, the cellulose surface of this dual-mode TMS material demonstrates high infrared transmittance within the atmospheric window, while the lignin surface exhibits advantageous absorption characteristics in the solar spectrum. This unique configuration empowers the material to achieve sub-ambient radiative cooling of 6 °C during the daytime and, when exposed to near-infrared illumination (808 nm, 1.0 W cm^{-2}), attain a photothermal conversion temperature exceeding 200 °C. Our comprehensive studies have validated that this thermoregulation effect can effectively save up to 22.86% of cooling and heating energy for a mid-rise building. Additionally, by capitalizing on the temperature differential generated during the photothermal conversion on the heating and cooling sides, we have incorporated a thermal-electric generator to produce electricity, capable of driving small electric fans. Furthermore, the dual-mode TMS material exhibits significant mechanical advantages over traditional structural materials such as pure wood fiber bulk. Its lightweight properties enable it to achieve twice the specific strength of hooked steel fiber concrete. Looking ahead, we envision integrating the dual-mode TMS material with an advanced system management model to enable more precise mode regulation based on seasonal temperature changes. This integration holds immense potential to substantially reduce carbon emissions and energy consumption, paving the way for future energy-efficient and sustainable building applications.

Author contributions

J. Z. performed the experiments and wrote the manuscript. K. Y. performed the cooling test and participated in the data discussion for actuation. Z. Z. and J. Z. participated in data characterization for the infrared (IR) spectra. Y. T. and J. X. took part in data recording for the photothermal test. Y. C. designed the experiments and revised the manuscript. Y. L. and Q. S. supervised the research.

Conflicts of interest

The authors declare no conflicts of interest.

Acknowledgements

The work was supported by National Natural Science Foundation of China [Grant No. 32371508] and the Scientific Research

Foundation of Zhejiang A&F University, China [Grant No. 2021FR032].

Notes and references

1 B. Song, H. Liang, R. Sun, P. Peng, Y. Jiang and D. She, *Int. J. Biol. Macromol.*, 2020, **144**, 219–230.
2 M. Isaac and D. P. Van Vuuren, *Energy Policy*, 2009, **37**, 507–521.
3 Q.-F. Guan, H.-B. Yang, Z.-M. Han, L.-C. Zhou, Y.-B. Zhu, Z.-C. Ling, H.-B. Jiang, P.-F. Wang, T. Ma and H.-A. Wu, *Sci. adv.*, 2020, **6**, eaaz1114.
4 X. Cao, X. Dai and J. Liu, *Energy Build.*, 2016, **128**, 198–213.
5 Y. Chen, B. Dang, J. Fu, C. Wang, C. Li, Q. Sun and H. Li, *Nano Lett.*, 2020, **21**, 397–404.
6 T. Li, Y. Zhai, S. He, W. Gan, Z. Wei, M. Heidarinejad, D. Dalgo, R. Mi, X. Zhao, J. Song, J. Dai, C. Chen, A. Aili, A. Vellore, A. Martini, R. Yang, J. Srebric, X. Yin and L. Hu, *Science*, 2019, **364**, 760–763.
7 D. H. Li, L. Yang and J. C. Lam, *Energy*, 2012, **42**, 103–112.
8 Y. Petri and K. Caldeira, *Sci. Rep.*, 2015, **5**, 1–14.
9 Y. Chen, B. Dang, J. Fu, C. Wang, C. Li, Q. Sun and H. Li, *Nano Lett.*, 2021, **21**, 397–404.
10 J. Li, W. Liu, X. Qiu, X. Zhao, Z. Chen, M. Yan, Z. Fang, Z. Li, Z. Tu and J. Huang, *Green Chem.*, 2022, **24**, 823–836.
11 Z. Tu, J. Wang, W. Liu, Z. Chen, J. Huang, J. Li, H. Lou and X. Qiu, *Mater. Horiz.*, 2022, **9**, 2613–2625.
12 X. Zhao, C. Huang, D. Xiao, P. Wang, X. Luo, W. Liu, S. Liu, J. Li, S. Li and Z. Chen, *ACS Appl. Mater. Interfaces*, 2021, **13**, 7600–7607.
13 Q. Shao, Y. Luo, M. Cao, X. Qiu and D. Zheng, *Chem. Eng. J.*, 2023, **476**, 146678.
14 Z. Chen, L. Zhu, W. Li and S. J. J. Fan, *Joule*, 2019, **3**, 101–110.
15 T. Li, Y. Zhai, S. He, W. Gan, Z. Wei, M. Heidarinejad, D. Dalgo, R. Mi, X. Zhao and J. Song, *Science*, 2019, **364**, 760–763.
16 H. Sun, C. Hou, T. Ji, X. Zhou, Z. Ren and Y. Song, *Compos. Part B*, 2023, **250**, 110426.
17 X. Shi, Y. Meng, R. Bi, Z. Wan, Y. Zhu and O. J. Rojas, *Compos. Part B*, 2022, **245**, 110231.
18 X. Dong, W. Gan, Y. Shang, J. Tang, Y. Wang, Z. Cao, Y. Xie, J. Liu, L. Bai and J. Li, *Nat. Sustainable*, 2022, 1–8, DOI: **10.1038/s41893-022-00887-8**.
19 S. Finland, 12cv – Municipal waste by treatment method in Finland, 2018-2022, **https://pxdata.stat.fi/PxWeb/pxweb/en/StatFin/StatFin__jate/statfin_jate_pxt_12cv.px/**, (accessed April 3rd, 2024).
20 J. Bolden, T. Abu-Lebdeh and E. Fini, *Am. J. Environ. Sci.*, 2013, **9**, 14–24.
21 N. Ijaz, F. Dai and Z. Ur Rehman, *J. Environ. Manage.*, 2020, **262**, 110285.
22 T. Saito, M. Hirota, N. Tamura, S. Kimura, H. Fukuzumi, L. Heux and A. Isogai, *Biomacromolecules*, 2009, **10**, 1992–1996.
23 S. Sun, S. Sun, X. Cao and R. J. B. T. Sun, *Bioresource Technol.*, 2016, **199**, 49–58.
24 A. Isogai, T. Saito and H. Fukuzumi, *Nanoscale*, 2011, **3**, 71–85.
25 J. Xu, R. Xia, L. Zheng, T. Yuan and R. J. C. P. Sun, *Carbohyd. Polym.*, 2019, **224**, 115164.
26 Y.-Y. Bai, Y.-H. Lei, X.-J. Shen, J. Luo, C.-L. Yao and R.-C. Sun, *Carbohyd. Polym.*, 2017, **174**, 610–616.
27 H. Zhao, Q. Sun, J. Zhou, X. Deng and J. Cui, *Adv. Mater.*, 2020, **32**, 2000870.
28 Y. Peng, L. Fan, W. Jin, Y. Ye, Z. Huang, S. Zhai, X. Luo, Y. Ma, J. Tang and J. Zhou, *Nat. Sustainable*, 2022, **5**, 339–347.
29 Y. Zhang and M. Naebe, *ACS Sustainable Chem. Eng.*, 2021, **9**, 1427–1442.
30 M. Jablonský, J. Kočiš, A. Ház and J. Šima, *Cell. Chem. Technol*, 2015, **49**, 267–274.
31 Y. Liu and P. Wu, *Adv. Sci.*, 2020, **7**, 2001269.
32 R. O. Ritchie, *Nat. Mater.*, 2011, **10**, 817.
33 S. E. Lebo Jr, J. D. Gargulak and T. J. McNally, *Encycl. Polym. Sci. Technol.*, 2002, **3**, 100–124.
34 A. Isogai, T. Saito and H. J. N. Fukuzumi, *Nanoscale*, 2011, **3**, 71–85.
35 P. O. Guglielmi, D. Blaese, M. P. Hablitzel, G. F. Nunes, V. R. Lauth, D. Hotza, H. A. Al-Qureshi and R. J. C. I. Janssen, *Ceram. Int.*, 2015, **41**, 7836–7846.
36 H.-B. Yao, H.-Y. Fang, X.-H. Wang and S.-H. Yu, *Chem. Soc. Rev.*, 2011, **40**, 3764–3785.
37 H. Zhu, S. Zhu, Z. Jia, S. Parvinian, Y. Li, O. Vaaland, L. Hu and T. Li, *P. Natl. A. Sci.*, 2015, **112**, 8971–8976.
38 Y. Chen, C. Sheng, B. Dang, T. Qian, C. Jin and Q. Sun, *ACS Appl. Mater. Interfaces*, 2018, **10**, 7344–7351.
39 Y. Chen, H. Wang, B. Dang, Y. Xiong, Q. Yao, C. Wang, Q. Sun and C. Jin, *Sci. Rep.*, 2017, **7**, 1–9.
40 H.-L. Gao, Y.-B. Zhu, L.-B. Mao, F.-C. Wang, X.-S. Luo, Y.-Y. Liu, Y. Lu, Z. Pan, J. Ge and W. J. N. C. Shen, *Nat. Commun.*, 2016, **7**, 12920.
41 Q. F. Guan, H. B. Yang, Z. M. Han, L. C. Zhou, Y. B. Zhu, Z. C. Ling, H. B. Jiang, P. F. Wang, T. Ma and H. Wu, *Sci. adv.*, 2020, **6**, eaaz1114.
42 M. Yoshimura, T. Nishioka, A. Yamakawa and M. Miyake, *J. Ceram. Soc. Jpn.*, 1995, **103**, 407–408.
43 S. Iqbal, A. Ali, K. Holschemacher and T. A. Bier, *Constr. Build. Mater.*, 2015, **98**, 325–333.
44 H. Su and J. Xu, *Constr. Build. Mater.*, 2013, **45** 306–313.
45 B. Chen, X. Peng, J.-G. Wang and X. Wu, *Ceram. Int.*, 2004, **30**, 2011–2014.
46 R. Yu, L. Van Beers, P. Spiesz and H. Brouwers, *Constr. Build. Mater.*, 2016, **107**, 203–215.
47 Y. Chen, J. Fu, B. Dang, Q. Sun, H. Li and T. Zhai, *ACS Nano*, 2020, **14**, 2036–2043.
48 E. S. Wibowo and B.-D. Park, *Molecules*, 2023, **28**, 2755.
49 Q. Shen, T. Zhang and M.-F. Zhu, *Colloids Surf., A*, 2008, **320**, 57–60.
50 A. P. Raman, M. A. Anoma, L. Zhu, E. Rephaeli and S. Fan, *Nature*, 2014, **515**, 540–544.
51 A. R. Gentle and G. B. Smith, *Adv. Sci.*, 2015, **2**, 1500119.

52 Y. Zou, X. Chen, P. Yang, G. Liang, Y. Yang, Z. Gu and Y. Li, *Sci. Adv.*, 2020, **6**, eabb4696.
53 Q. Sun, Y. Lu, H. Zhang, H. Zhao, H. Yu, J. Xu, Y. Fu, D. Yang and Y. J. M. C. Liu, *Mater. Chem. Phys.*, 2012, **133** 253–258.
54 M. Deru, K. Field, D. Studer, K. Benne, B. Griffith, P. Torcellini, B. Liu, M. Halverson, D. Winiarski and M. Rosenberg, *U.S. Department of Energy Commercial Reference Building Models of the National Building Stock*, 2011, p. 118, DOI: 10.2172/1009264.

